Available online at www.sciencedirect.com

ScienceDirect

Procedia CIRP 00 (2018) 000–000

www.elsevier.com/locate/procedia

8th CIRP Conference on High Performance Cutting (HPC 2018)

On process damping induced by vibration-dependency of cutting direction in milling

Tamas G. Molnar[a,*], Daniel Bachrathy[a], Tamas Insperger[b], Gabor Stepan[a]

[a] *Department of Applied Mechanics, Budapest University of Technology and Economics, H-1111 Budapest, Hungary*

[b] *Department of Applied Mechanics, Budapest University of Technology and Economics and MTA-BME Lendület Human Balancing Research Group, H-1111 Budapest, Hungary*

* Corresponding author. *E-mail address:* molnar@mm.bme.hu

Abstract

The process damping effect is analyzed for regenerative machine tool chatter in milling via a velocity-dependent cutting force model. This model takes into account that the effective cutting direction depends on the vibrations of the machine tool-workpiece system, which modifies the effective rake angle, the chip thickness, and the cutting force. The model was originally introduced for turning operations where it results in a process damping term that improves the stability of metal cutting at low cutting speeds. Now this model is extended to milling. It is shown that the vibration-dependency of the cutting direction induces a time-periodic process damping term that is negative when the radial immersion is low. This decreases the stability at low cutting speeds, thus the low-speed stability improvement phenomenon in low radial immersion milling can be explained by extended process damping models only.

Peer-review under the responsibility of the International Scientific Committee of the 8th CIRP Conference on High Performance Cutting (HPC 2018).

Keywords: milling, dynamics, machine tool chatter, process damping

1. Introduction

This paper is devoted to the stability analysis of delay-differential equations describing milling in order to predict harmful vibrations (chatter) during metal cutting. Milling experiments reported in the literature [1–6] have shown that the maximum chatter-free axial depth of cut typically increases for decreasing spindle speed. We call this *low-speed stability improvement phenomenon*. The phenomenon is often explained by an additional damping – called *process damping* – which is inversely proportional to the spindle speed [1–8]. Most papers dedicate process damping to the interference between the tool's flank face and the wavy surface finish [1–7], while in other models velocity-dependent chip thickness and cutting force expressions give rise to process damping [2,8]. Alternatively, the low-speed stability improvement can be explained by the distribution of the cutting force along the tool's rake face [9–11].

In [2,8], process damping is explained for turning by taking into account the fluctuation of the cutting direction due to the vibrations of the tool. This effect results in velocity-dependent chip thickness and cutting force expressions [12,13]. Now these results are extended by recognizing that the cutting direction affects the effective rake angle, which leads to velocity-dependent cutting-force coefficients.

2. Mechanical model of milling

We investigate the single-degree-of-freedom model of milling shown in Fig. 1a, where the tool is rigid and the workpiece is compliant in the feed direction x. Using the modal mass m, the undamped natural angular frequency ω_n, and the damping ratio ζ, the motion of the workpiece is described by

$$\ddot{x}(t) + 2\zeta\omega_\mathrm{n}\dot{x}(t) + \omega_\mathrm{n}^2 x(t) = -\frac{1}{m}F_x(t)\,. \tag{1}$$

Here, $F_x(t)$ is the x-directional component of the cutting force acting on the mill, which is associated with the cutting velocity and the chip thickness at the cutting edges.

Consider an N-fluted tool of radius R rotating with angular velocity Ω. The angular position of the jth tooth is $\tilde{\varphi}_j(t) = \Omega t + (j-1)2\pi/N$. If the feed velocity is negligible, $\tilde{\varphi}_j(t)$ describes the direction of the nominal cutting velocity $\tilde{\mathbf{v}}_j(t)$ of magnitude $R\Omega$ (see Fig. 1b). This direction is the nominal tangential direction $\tilde{t}_j$, the perpendicular one is the nominal radial direction $\tilde{r}_j$.

When machine tool vibrations occur, the vibration velocity $\dot{x}(t)$ modifies the velocity of the jth cutting edge and the cutting (tangential) direction. The magnitude $v_j(t)$ and direction $\varphi_j(t)$

Peer-review under the responsibility of the International Scientific Committee of the 8th CIRP Conference on High Performance Cutting (HPC 2018).

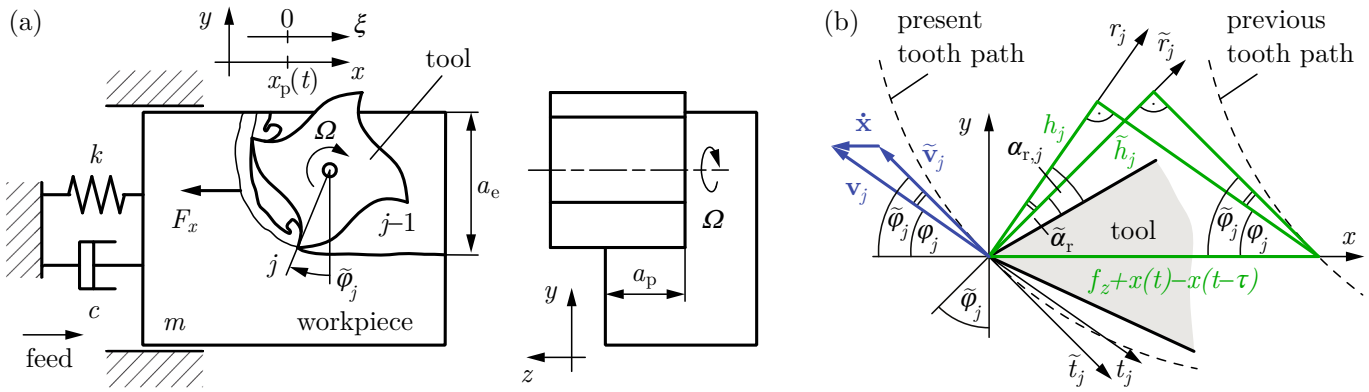

Fig. 1. The mechanical model of milling (a); the illustration of the cutting velocity, chip thickness, and rake angle (b).

of the actual cutting velocity are given by

$$v_j(t) = \sqrt{\left(R\Omega\cos\tilde{\varphi}_j(t) + \dot{x}(t)\right)^2 + \left(R\Omega\sin\tilde{\varphi}_j(t)\right)^2}\,,$$
$$\cos\varphi_j(t) = \frac{R\Omega\cos\tilde{\varphi}_j(t) + \dot{x}(t)}{v_j(t)}\,,\quad \sin\varphi_j(t) = \frac{R\Omega\sin\tilde{\varphi}_j(t)}{v_j(t)}\,. \tag{2}$$

Note that quantities related to the nominal cutting velocity are indicated by tilde, while those without tilde (such as directions t_j and r_j in Fig. 1b) correspond to the actual cutting velocity.

Since the angle of the cutting direction changes from $\tilde{\varphi}_j(t)$ to $\varphi_j(t)$ during chatter, the rake angle is modified from the nominal value $\tilde{\alpha}_\mathrm{r}$ to the actual value $\alpha_{\mathrm{r},j}(t) = \tilde{\alpha}_\mathrm{r} + \tilde{\varphi}_j(t) - \varphi_j(t)$, cf. Fig. 1b. The fluctuations of the cutting direction also affect the actual chip thickness $h_j(t)$, which is the projection of the feed per tooth to the actual radial direction. For prescribed feed per tooth f_z and tooth passing period $\tau = 2\pi/(N\Omega)$, the instantaneous feed per tooth becomes $f_z + x(t) - x(t-\tau)$, and we can write

$$h_j(t) = \left(f_z + x(t) - x(t-\tau)\right)\sin\varphi_j(t)\,, \tag{3}$$

cf. Fig. 1b. Note that the actual chip thickness $h_j(t)$ is velocity dependent, since $\varphi_j(t)$ depends on $\dot{x}(t)$ as shown by Eq. (2).

3. Cutting Force Model

For reference, consider first orthogonal cutting with a linear cutting force model: $F_x(t) = K_x a h(t)$, where a denotes the chip width and K_x is the feed-directional cutting-force coefficient. It is well-known that cutting-force coefficients strongly depend on the rake angle $\tilde{\alpha}_\mathrm{r}$. According to Eqs. (2.42) and (2.47) of [8],

$$K_x = \tau_\mathrm{s}\frac{\sin\left(\beta_\mathrm{a} - \tilde{\alpha}_\mathrm{r}\right)}{\sin\Phi\cos\left(\Phi + \beta_\mathrm{a} - \tilde{\alpha}_\mathrm{r}\right)}\,, \tag{4}$$

where β_a is the average friction angle and τ_s is the shear stress along the shear plane located at angle $\Phi = \pi/4 - (\beta_\mathrm{a} - \tilde{\alpha}_\mathrm{r})/2$. The cutting-force coefficient K_x is shown in Fig. 2 as a function of the rake angle $\tilde{\alpha}_\mathrm{r}$ for various friction coefficients $\mu = \tan\beta_\mathrm{a}$.

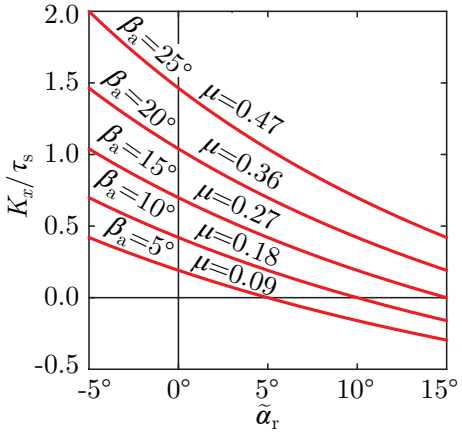

Fig. 2. The effect of the rake angle on the cutting-force coefficients [8].

The cutting-force coefficient becomes negative for large rake angles, which has key importance in the subsequent analysis of milling with vibration-induced fluctuation of the rake angle.

Now the cutting-force coefficients are derived for milling following [8] via Merchant's circle shown in Fig. 3. The cutting force $\mathbf{F}_j$ on the jth cutting edge is decomposed into four component pairs: x and y-directional ($\mathbf{F}_{j,x}$, $\mathbf{F}_{j,y}$); actual tangential and radial ($\mathbf{F}_{j,\mathrm{t}}$, $\mathbf{F}_{j,\mathrm{r}}$); parallel and normal to the rake face ($\mathbf{F}_{j,u}$, $\mathbf{F}_{j,v}$); parallel and normal to the shear plane ($\mathbf{F}_{j,\mathrm{s}}$, $\mathbf{F}_{j,\mathrm{n}}$).

Following [8], the shear stress τ_s along the shear plane located at shear angle $\Phi_j(t)$ is assumed to be constant during cutting. Therefore, the cutting force component $F_{j,\mathrm{s}}(t)$ is the product of the shear stress and the shear plane area:

$$F_{j,\mathrm{s}}(t) = g_j(t)\tau_\mathrm{s}a_\mathrm{p}\frac{h_j(t)}{\sin\Phi_j(t)}\,, \tag{5}$$

$$g_j(t) = \begin{cases} 1 & \text{if } \varphi_\mathrm{en} < (\tilde{\varphi}_j(t) \bmod 2\pi) < \varphi_\mathrm{ex}\,, \\ 0 & \text{otherwise.} \end{cases} \tag{6}$$

Here, $g_j(t)$ is a screen function that indicates whether the jth tooth is currently engaged in cutting, mod is the modulo function, while φ_en and φ_ex are the enter and exit immersion angles.

The angle between the cutting force $\mathbf{F}_j(t)$ and the rake face normal is the average friction angle β_a, which is assumed to be constant. The cutting force magnitudes $F_j(t)$ and $F_{j,x}(t)$ can be obtained from $F_{j,\mathrm{s}}(t)$ by considering the rectangular triangles in

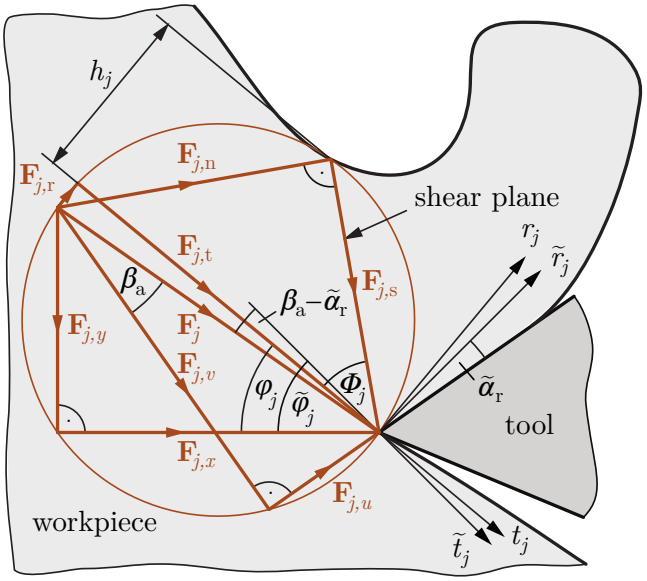

Fig. 3. Merchant's circle representing the components of the cutting force.

Fig. 3. Summing the forces on each tooth of the mill leads to

$$F_x(t) = \sum_{j=1}^{N} g_j(t) K_{j,x}(t) a_p h_j(t)\,, \tag{7}$$

$$K_{j,x}(t) = \frac{\tau_s \cos\left(\tilde{\varphi}_j(t) - (\beta_a - \tilde{\alpha}_r)\right)}{\sin\Phi_j(t)\cos\left(\Phi_j(t) + \varphi_j(t) - \tilde{\varphi}_j(t) + \beta_a - \tilde{\alpha}_r\right)}\,. \tag{8}$$

Note that the coefficient $K_{j,x}(t)$ depends on the vibration velocity $\dot{x}(t)$ through the cutting direction $\varphi_j(t)$, which determines the effective rake angle $\tilde{\alpha}_r + \tilde{\varphi}_j(t) - \varphi_j(t)$. If a single tooth is cutting at position $\tilde{\varphi}_j(t) = 90°$ and no machine tool vibrations arise ($\dot{x}(t) = 0$, $\varphi_j(t) = \tilde{\varphi}_j(t)$), we get Eq. (4) of orthogonal cutting.

As for the shear angle $\Phi_j(t)$, one widely used model is the minimum energy principle (MEP) [8]. The MEP calculates the shear angle such that the power $-F_{j,t}(t)v_j(t)$ of the cutting force is minimal, which leads to

$$\Phi_j(t) + \frac{\varphi_j(t) - \tilde{\varphi}_j(t) + \beta_a - \tilde{\alpha}_r}{2} = \frac{\pi}{4}\,. \tag{9}$$

Note that Eqs. (2) and (9) imply velocity-dependent shear angle.

4. Linearized equation of motion

Equations (1) and (7) define a nonlinear delay-differential equation, since the relationship between $\varphi_j(t)$ and $\dot{x}(t)$ is nonlinear (see Eq. (2)). The differential equation has a periodic solution $x_p(t) = x_p(t+\tau)$ that corresponds to stationary cutting. The instability of this solution determines the onset of chatter.

In order to analyze linear stability, let us linearize Eq. (1) around the solution $x_p(t)$:

$$\ddot{\xi}(t) + 2\zeta\omega_n\dot{\xi}(t) + \omega_n^2\xi(t) = -\frac{1}{m}\left(\frac{\partial F_x}{\partial x}\bigg|_p (\xi(t) - \xi(t-\tau)) + \frac{\partial F_x}{\partial \dot{x}}\bigg|_p \dot{\xi}(t)\right), \tag{10}$$

where $\xi(t)$ is a small perturbation added to the solution $x_p(t)$, and subscript p stands for the substitution $x(t) = x_p(t)$.

Substitution of Eq. (7) into Eq. (10) leads to the form

$$\ddot{\xi}(t) + 2\zeta\omega_n\dot{\xi}(t) + \omega_n^2\xi(t) = -HG_1(t)\left(\xi(t) - \xi(t-\tau)\right) - \frac{Hf_z}{R\Omega}G_2(t)\dot{\xi}(t). \tag{11}$$

Provided that the velocity $\dot{x}_p(t)$ is negligible compared to the nominal cutting speed $R\Omega$, the specific cutting-force coefficient is $H = C_0 a_p/m$ and the τ-periodic coefficients $G_1(t)$, $G_2(t)$ are

$$\begin{aligned} G_1(t) &= \sum_{j=1}^{N} g_j(t)\left(C_1\cos\tilde{\varphi}_j(t) + \sin\tilde{\varphi}_j(t)\right)\sin\tilde{\varphi}_j(t)\,, \\ G_2(t) &= -\sum_{j=1}^{N} g_j(t)\left(C_1\cos\tilde{\varphi}_j(t) + \sin\tilde{\varphi}_j(t)\right)\sin\tilde{\varphi}_j(t) \\ &\quad\times\left(\cos\tilde{\varphi}_j(t) + C_2\sin\tilde{\varphi}_j(t)\right) \end{aligned} \tag{12}$$

with the following constants for the MEP shear angle model

$$C_0 = \frac{2\tau_s\sin(\beta_a - \tilde{\alpha}_r)}{1 - \sin(\beta_a - \tilde{\alpha}_r)}\,, \quad C_1 = \cot(\beta_a - \tilde{\alpha}_r)\,, \quad C_2 = \frac{C_0 C_1}{2\tau_s}\,. \tag{13}$$

Note that in standard velocity-independent cutting force models, H and $G_1(t)$ are given by $C_0 = K_r$ and $C_1 = K_t/K_r$, where K_t and K_r are the (nominal) tangential and radial cutting-force coefficients [14]. The last term in Eq. (11) is absent from standard models [14–16]. This term implies an additional damping that is inversely proportional to the spindle speed, known as process damping. Most models use constant process damping [1–8], while now it is time-periodic through $G_2(t)$. This affects the stability lobe diagrams of milling significantly.

5. Stability lobe diagrams and conclusions

Figure 4 shows an example with $N = 2$ flutes, damping ratio $\zeta = 0.02$, friction angle $\beta_a = 20°$, and rake angle $\tilde{\alpha}_r = 0°$. Two cases (A and B) are presented, where the enter and exit angles are $\varphi_{en}^A = 0°$, $\varphi_{ex}^A = 30°$ (up-milling) and $\varphi_{en}^B = 110°$, $\varphi_{ex}^B = 145°$ (down-milling). The periodic coefficients $G_2^A(t)$, $G_2^B(t)$ given by Eq. (12) are indicated by red and green lines in Fig. 4a. These can be obtained from the one describing full-immersion milling ($\varphi_{en} = 0°$, $\varphi_{ex} = 180°$; see solid black line), by multiplying it with the screen functions $g^A(t)$ and $g^B(t)$ shown at the bottom.

Figures 4b and 4c show the stability lobe diagrams of cases A and B, which were obtained by the semi-discretization method [14] for a 600×300 grid in the parameter plane with 150 intervals of delay resolution. Dashed lines show the stability boundaries of standard models without process damping ($G_2(t) \equiv 0$) whose lower envelope is a horizontal straight line. Solid lines show the effect of the time-periodic process damping

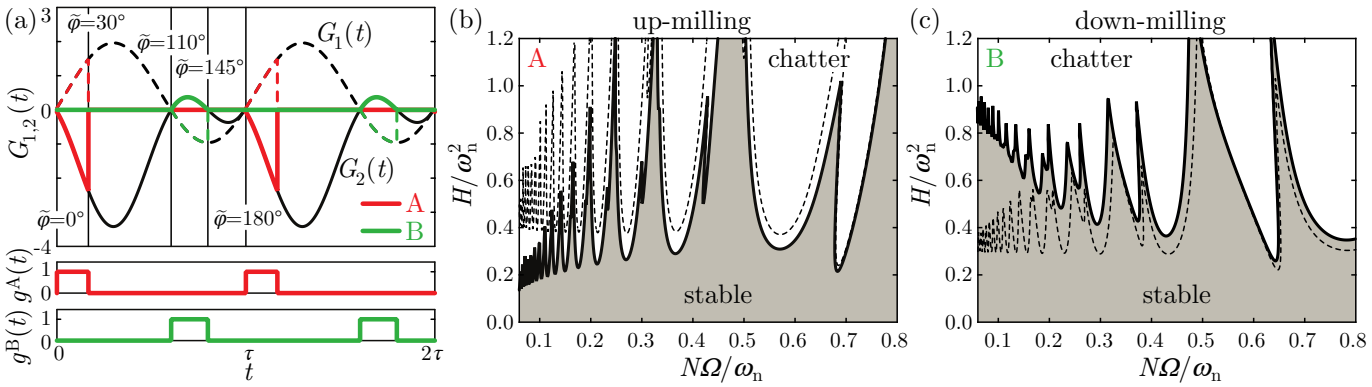

Fig. 4. The coefficients $G_1(t)$ of the delayed term and $G_2(t)$ of process damping (a); the corresponding stability charts for two different cutting conditions (b,c).

in Eq. (11) for dimensionless feed per tooth $f_z N/(2R\pi) = 0.01$ and 0.05 in cases A and B, respectively. In case B, the process damping coefficient $G_2(t)$ is always nonnegative, thus the stability lobes shift upwards at low spindle speeds similarly to the models of constant process damping [1–8]. In case A, $G_2(t)$ takes negative values, and the stability lobes shift downwards with a decrease in low-speed stability instead of improvement.

Note that for a two-fluted tool, a single tooth is engaged in cutting at any time. In such cases, the process damping is negative ($G_2(t) < 0$) at certain angular positions of the teeth according to Eq. (12). Process damping is negative if cutting takes place within angular positions 0° and $\pi/2 + \beta_a - \tilde{\alpha}_r = 110°$, which involves up-milling processes; or within angular positions $3\pi/4 + (\beta_a - \tilde{\alpha}_r)/2 = 145°$ and 180°, which implies low radial immersion down-milling. Process damping is negative also for $\tilde{\varphi}_j(t) \equiv 90°$, i.e., for orthogonal cutting. In these cases, the chatter-free technological parameter region shrinks for low cutting speeds. Note that the sign of process damping is also affected by the modal direction (which was now assumed to be the feed direction x) and the corresponding directional factor.

In conclusion, the vibration-induced fluctuations of the cutting direction act against the low-speed stability improvement phenomenon for orthogonal cutting and low-immersion milling. In order to explain the phenomenon for any cutting condition, one may introduce improved models for the shear angle or the friction angle (see an example in [17]). An alternative explanation is the interference between the tool's flank face and the wavy surface of the workpiece [1–7]. Since the flank contact is intermittent, this in fact yields complicated non-smooth dynamics [7] that cannot be described by linear models including constant process damping. A different approach is considering the distribution of the cutting force along the tool's rake face [9,10], which improves low-speed stability both for turning [9,10] and for milling with any radial immersion [11].

Our future research involves the experimental investigation of process damping via chatter tests in milling and the measurement of cutting forces during fluctuating the cutting direction in orthogonal cutting.

Acknowledgements

The research leading to these results has received funding from the European Research Council under the European Union's Seventh Framework Programme (FP/2007-2013) / ERC Advanced Grant Agreement n. 340889.

References

[1] Clancy, B.E., Shin, Y.C.. A comprehensive chatter prediction model for face turning operation including tool wear effect. Int J Mach Tool Manu 2002;42(9):1035–1044.
[2] Altintas, Y., Eynian, M., Onozuka, H.. Identification of dynamic cutting force coefficients and chatter stability with process damping. CIRP Ann - Manuf Techn 2008;57(1):371–374.
[3] Budak, E., Tunc, L.T.. Identification and modeling of process damping in turning and milling using a new approach. CIRP Ann - Manuf Techn 2010;59(1):403–408.
[4] Ahmadi, K., Ismail, F.. Stability lobes in milling including process damping and utilizing multi-frequency and semi-discretization methods. Int J Mach Tool Manu 2012;54–55:46–54.
[5] Tyler, C.T., Schmitz, T.L.. Analytical process damping stability prediction. J Manuf Process 2013;15(1):69–76.
[6] Jin, X.. Identification of process damping coefficient based on material constitutive property. In: Proc of the ASME International Manufacturing Science and Engineering Conference. MSEC2014–4204; Detroit, MI, USA; 2014, p. 1–7.
[7] Bachrathy, D., Stépán, G.. Time-periodic velocity-dependent process damping in milling processes. In: Altintas, Y., Denkena, B., Brecher, C., editors. Proc of the 2nd International CIRP Conference on Process Machine Interaction. Vancouver, Canada; 2010, p. 1–12.
[8] Altintas, Y.. Manufacturing Automation - Metal Cutting Mechanics, Machine Tool Vibrations and CNC Design, Second Edition. Cambridge: Cambridge University Press; 2012.
[9] Stépán, G.. Delay-differential equation models for machine tool chatter. In: Moon, F.C., editor. Dynamics and Chaos in Manufacturing Processes. New York: John Wiley and Sons; 1997, p. 165–192.
[10] Dombóvári, Z., Stépán, G.. Experimental and theoretical study of distributed delay in machining. In: Proc of the 9th IFAC Workshop on Time Delay Systems. Prague, Czech Republic; 2010, p. 1–5.
[11] Molnár, T.G., Insperger, T.. On the effect of distributed regenerative delay on the stability lobe diagrams of milling processes. Period Polytech Mech 2015;59(3):126–136.
[12] Bachrathy, D., Stépán, G.. Bistable parameter region caused by velocity dependent chip thickness in milling process. In: Proc of the 12th CIRP Conference on Modelling of Machining Operations. San Sebastian, Spain; 2009, p. 867–871.
[13] Molnár, T.G., Insperger, T., Bachrathy, D., Stépán, G.. Extension of process damping to milling with low radial immersion. Int J Adv Manuf Tech 2017;89(9):2545–2556.
[14] Insperger, T., Stépán, G.. Semi-Discretization for Time-Delay Systems - Stability and Engineering Applications. New York: Springer; 2011.
[15] Altintas, Y., Budak, E.. Analytical prediction of stability lobes in milling. CIRP Ann - Manuf Techn 1995;44(1):357–362.
[16] Faassen, R.P.H., van de Wouw, N., Oosterling, J.A.J., Nijmeijer, H.. Prediction of regenerative chatter by modelling and analysis of high-speed milling. Int J Mach Tool Manu 2003;43(14):1437–1446.
[17] Chandiramani, N.K., Pothala, T.. Dynamics of 2-dof regenerative chatter during turning. J Sound Vib 2006;290(1–2):448–464.